

Beam Models for Gamma-Ray Bursts Sources: Outflow Structure, Kinematics and Emission Mechanisms

Enrico Ramirez-Ruiz¹

Institute of Astronomy, Madingley Road, Cambridge, CB30HA, England

and

Nicole M. Lloyd-Ronning²

*Canadian Institute of Theoretical Astrophysics, 60 St. George Street, Toronto, M5S 3H8,
Canada*

Abstract

The variety of γ -ray burst phenomenology could be largely attributable to differences in the opening angle of an isotropic outflow or to a standard type of event viewed from different orientations. Motivated by this currently popular idea, we study the effects of varying the energy per unit solid angle in the unsteady expelled outflow by an increase either in the bulk Lorentz factor or in the baryon loading. We apply these models to interpret the observed correlations between variability, luminosity and spectral peak energy and find that while the latter scenario fails to provide a good description, bursts produced by collisions between similar mass shells but with increasingly large Lorentz factors are both more variable and have larger peak spectral energies. We present detailed internal shock calculations confirming this interpretation and discuss the roles various timescales, radii and the optical thickness of the wind play in determining this wide range of behaviors. Finally, we discuss the variety of scenarios in which large variations of the source expansion velocity are naturally expected.

Key words:

gamma rays: bursts — Stars: evolution – methods:numerical–radiation mechanisms: non thermal – stars: supernovae

PACS: 04.70.Bw, 95.30.Lz, 95.30.Qd, 97.60.Bw

¹ E-mail: enrico@ast.cam.ac.uk

² E-mail: lloyd@cita.utoronto.ca

1 Introduction

The discovery of afterglows in recent years (Costa et al. 1997; van Paradijs et al. 1997; Frail et al. 1997) has moved the study of gamma-ray bursts (GRB) to a new plane. It not only has extended observations to longer timescales and other wavelength bands, enabling the measurement of redshift distances, but has also provided a direct determination of the source size and confirmation of its relativistic expansion (see Piran 1999 and Mészáros 2001 for recent reviews). Detailed predictions of the afterglow properties, made in advance of the observations (Mészáros & Rees 1997; Vietri 1997), agreed well with subsequent detections at these wavelengths, followed over timescales of months. While progress has been made in understanding how the GRB and afterglow radiation arises in terms of an unsteady relativistic outflow followed by the development of a blast wave moving into the external medium, interest continues to grow as new observations provided new challenges of interpretation.

Many GRBs are now found to be associated with star forming regions (Kulkarni et al. 1998; Fruchter et al. 1999; Berger, Kulkarni & Frail 2001), the remnants of a massive stellar progenitor system (Piro et al. 2000; Amati et al. 2000) and possibly supernovae (Galama et al. 1998; Bloom et al. 1999; Reichart 1999; Björnsson et al. 2001; Lazzati et al. 2001b). These observations give support to the idea that the most common GRBs could be linked to the collapse of massive stars (Woosley 1993; Paczyński 1998; MacFadyen & Woosley 1999). This speculation is made more intriguing by the recent report that GRBs could be highly collimated, so that there may be many more events Doppler boosted in directions other than ours, bringing the GRB rate to within a factor of 100 or so of the supernova rate and their derived explosive bulk energies down to $\approx 10^{52.5}$ erg (Frail et al. 2001, Panaitescu & Kumar 2001; Piran et al. 2001; assuming a conversion efficiency of 1%). The apparent dispersion in isotropic energies is then caused by a distribution of jet opening angles – bursts with higher energy per solid angle are more collimated (or maybe viewed closer to the jet axis; see Rossi, Lazzati & Rees 2002; Salmonson & Galama 2002; Zhang & Mészáros 2002). New evidence and new puzzles were added when the total isotropic luminosity was found to be also related with a variety of temporal and spectral behaviors exhibited by γ -ray light curves - namely the degree of variability or “spikiness” (Fenimore & Ramirez-Ruiz 2002a), the differential time lags for the arrival of burst pulses at different energies (Norris, Marani & Bonnell 2000, Norris 2002), and the rest frame GRB peak energy (Lloyd-Ronning & Ramirez-Ruiz 2002).

These correlations are still tentative, but if confirmed they could be used to relate the properties of material moving almost directly towards us (e.g. the variable activity of the γ -ray light curve) with the ejection in directions away from our line of sight (e.g. degree of collimation; see Salmonson 2000; Ioka & Nakamura 2001; Kobayashi et al. 2002; Plaga 2001). This could turn out to be very important, since

at present we can only infer the energy per solid angle; as yet the constraints on the angle-integrated γ -ray energy are not strong. The gamma-rays we receive come only from material whose motion is directed within $1/\Gamma$ of our line of sight. They therefore provide no information about the ejecta in other directions. At observer times of more than a week, the beaming and aberration effects are less extreme so we observe afterglow emission from a wider range of angles. At these later times, however, all memory of the initial time-structure of the outflow responsible for the γ -ray emission would be lost.

Information regarding how much energy and momentum has been injected, its distribution in angle, the mass fractions in shells with different Lorentz factors and its efficiency in radiated gamma-rays are at the forefront of attention. We address some aspects of these issues here by studying the physical conditions under which simulated GRBs arising from internal shocks in relativistic winds can account for this burst phenomenology - degree of collimation, variable γ -ray activity, the rest frame peak energy and the total burst luminosity. To that effect, we consider anisotropic relativistic outflows where changes in the energy per solid angle are caused either by an increase in the bulk Lorentz factor or in the baryon loading. We apply these models to interpret the large variety of behaviors exhibited by both the afterglow and the prompt emission, and discuss their possible use for predicting the internal structure of the collimated outflow. Some possible scenarios in which large variations of the energy per solid angle are naturally expected are highlighted, along with the types of observation that would discriminate among the various models. We assume $H_0 = 65 \text{ km s}^{-1} \text{ Mpc}^{-1}$, $\Omega_{\text{matter}} = 0.3$, and $\Omega_{\Lambda} = 0.7$.

2 Anisotropic or Highly Beamed Outflows?

The high Lorentz factors and energies seen in GRBs are consistent with the catastrophic formation of a stellar black hole of a few M_{\odot} , with $\approx 1\%$ going to a relativistic outflow. This could be the extreme example of the asymmetric explosion produced by supernova (Khokhlov et al. 1999), in which instead of halting at the neutron star stage, the collapse continues to the black-hole stage, producing an even faster jet in the process (MacFadyen & Woosley 1999). GRBs arising from a very small fraction of stars that undergo this type of catastrophic energy release are likely to produce collimated outflows.

Even if the outflow is not highly collimated, some beaming is expected because energy would be channeled preferentially along the rotation axis. Also, one would expect baryon contamination to be lowest near the axis, because angular momentum flings material away from the axis and material with low-angular momentum falls into the black hole. The dynamics, however, are complex. While numerical simulations of collapse scenarios can address the fate of the bulk of the matter (MacFadyen &

Woosley 1999; MacFadyen, Woosley & Heger 2001; Aloy et al. 2000; Zhang et al. 2002, in preparation), higher resolution simulations of the outer layers of the stellar mantle seem to be required since even a very small amount of baryons polluting the outflow could severely limit the attainable Lorentz factor. It is quite possible, for instance, that the stellar pressure will tend to collimate the fireball into a jet. A broad spread of Lorentz factors is thus expected – close to the rotation axis Γ may be high. At larger angles away from the jet axis, there may be an increasing degree of entrainment, with a corresponding decrease in Γ . So in this model, the measured flux is more intense when observed closer to the jet axis (with an angle $\theta_v \approx 0$ from the jet axis). A large spread in the inferred luminosities thus originates from the differences in viewing angles (see Figure 1a). This interpretation may be appealing because a large spread of both Lorentz factors and luminosities could be attributable to a standard type of event viewed from different orientations (Rees 1999). On the other hand, the large variations in the fluences of GRB could also originate from differences in the opening angle θ_j of an isotropic outflow (see Figure 1b; Frail et al. 2001; Panaitescu & Kumar 2001; Piran et al. 2001). The dynamics of the blast-wave in the off-axis anisotropic jet are almost indistinguishable from the uniform jet model, provided that the energy per unit solid angle varies as $\theta_{v,j}^{\approx -2}$ (Kobayashi et al. 2002; Rossi et al. 2002; Salmonson & Galama 2002; Zhang & Mészáros 2002).

The correlations between variability, the luminosity per unit solid angle and the characteristic photon energy in the cosmological rest frame (Lloyd-Ronning & Ramirez-Ruiz 2002) impose severe restrictions on any emission model. The question at hand is whether this burst phenomenology, combined with the intrinsic variations in energy per unit solid angle discussed above, can be understood in terms of internal shocks and if so, under what conditions. To this end, the results presented in §3 are independent of whether the variations in energy per unit solid angle are caused either by the viewing angle of a standard event (provided that $d\Gamma/d\theta_v$ is small for $d\theta_v \leq \Gamma^{-1}$) or by collimated jets, in which the typical Lorentz factor (or energy per unit solid angle) is higher when the jet is highly collimated.

2.1 *Highly collimated outflows*

As discussed above, the gamma-rays we receive come only from material whose motion is directed within an angle Γ^{-1} of our line of sight. At observer times of more than a week, the shocked outflow starts to slow down. As Γ drops after the deceleration shock, the causal angle includes an increasing amount of the solid angle toward the jet as well as towards the equator, so we observe emission from a wider range of angles. The afterglow is thus a direct probe of the geometry of the ejecta – if the outflow is beamed, we expect a downturn in the light curve as the edge of the jet becomes visible (Rhoads 1997). Collimation factors of $\Omega_j/4\pi < 0.01$ have been

derived from the observation of such steepenings³ (Kulkarni et al. 1999; Castro-Tirado et al. 1999; Harrison et al. 1999; Frail et al. 2001; Panaitescu & Kumar 2001). Although several methods of producing and collimating jets have been proposed, these highly collimated outflows of plasma with velocities close to the speed of light may be a unique feature of rapidly rotating, gravitationally confined plasmas that are threaded by a strong magnetic field (e.g. Uchida & Shibata 1985). An important result from present numerical simulations of Poynting flux-dominated outflows, which was not predicted by semi-analytical steady state studies, is that the jets arising from these outflows are likely to be highly collimated (see Meier, Koide & Uchida 2001 for a recent review). Because of the strong pinch that develops, a narrow jet that delivers its thrust in a narrow solid angle may be a common ingredient of strong rotating magnetic fields, not only for accretion disks but also perhaps for many jet-producing objects.

The range of parameter space where high jet speeds are expected (i.e. jets propelled at speeds much larger than the local escape velocity) is determined by the condition $L_{\text{MHD}} \geq L_C$. The MHD luminosity

$$L_{\text{MHD}} = \frac{B_p^2 R_0^4 \Omega_0^2}{32c} \quad (1)$$

depends only on the poloidal magnetic field B_p protruding from the jet-production region at radius R_0 and on the angular velocity of the field Ω_0 (Blandford & Znajek 1977), while the critical luminosity L_C is defined to be that given by the ratio between the energy needed for the plasma to reach the escape velocity and the free-fall time,

$$L_C = 4\pi R_0^2 \rho_0 \left(\frac{GM}{R_0} \right)^{3/2}, \quad (2)$$

where ρ_0 is the density of the plasma. The condition $L_{\text{MHD}} \geq L_C$ is a necessary requirement to explain the $\Gamma > 100$ outflow seen in GRBs, even from the vicinity of black holes. This criterion is similar to that of LeBlanc and Wilson 1970, in which the magnetic field grows to a dynamically important value in less than a dynamical time, which seems to be a condition of forming MHD jets in collapsing supernova cores (Meier et al. 1976; Wheeler et al. 1999). Although carrying more power, these highly collimated outflows will be much less efficient in imparting

³ The above argument assumes that the breaks observed in many GRB afterglow light-curves are due to a geometrical beam effect and not to either a transition to non-relativistic expansion (Huang, Dai & Lu 2000) or an environmental effect such as a sharp density gradient (Chevalier & Li 2000; Ramirez-Ruiz et al. 2001). An important feature produced by this jet collimation is the achromaticity of the afterglow break, which will clearly distinguish it from the steepening that may be produced by the passage of a spectral break through the observing band.

energy and momentum to the outer stellar layers and may not explode (Khokhlov et al. 1999). These failed explosions may be similar to the failed supernova model for GRBs (MacFadyen & Woosley 1999), continuing to accrete much of the stellar mantle and thus collapsing into a black hole.

While the very narrow $\approx 2^\circ$ and fast jets $\Gamma > 100$ that are speculated to exist in γ -ray bursts (Panaitescu & Kumar 2001) may be a general feature of strong rotating magnetic fields, some observations may be difficult to reconcile with this interpretation. For example, several afterglows have shown evidence of large amount of X-ray line emitting material, possibly arising from ionized iron (Piro et al. 1999; Yoshida et al. 1999; Piro et al. 2000; Antonelli et al. 2000). The large Fe $K\alpha$ equivalent widths inferred from the X-ray observations favor models in which the line is produced when the primary X-ray emission from the source strikes Thomson-thick material and Compton scatters into our line of sight (Lazzati, Campana & Ghisellini 1999; Böttcher & Fryer 2000; Vietri et al. 2000; Rees & Mészáros 2000; Ballantyne & Ramirez-Ruiz 2001, Lazzati et al. 2001). These conditions impose strong constraints on the location and geometry of the optically thick reflecting material, as well as on the structure of the outflow producing the primary X-rays - illumination of the stellar remnant may be complicated if the GRB emission is highly beamed. This problem may be overcome in particular source geometries for which lower luminosities and softer spectra are expected at the edges of the relativistic outflow (Ballantyne & Ramirez-Ruiz 2001). More importantly, highly collimated outflows bring the GRB rate to within a factor of 100 or so of the supernova rate (Frail et al. 2001). Those stars that produce GRBs are likely to have core masses $> 6M_\odot$ at the time they collapse (Woosley 1993). Stars satisfying this criterion are $\approx 30-50$ times rarer than those producing SN Ib/c (Izzard, Ramirez-Ruiz & Tout 2002, in preparation). Because burst formation is also likely to be favored by rapid rotation and low metallicity (MacFadyen & Woosley 1999), highly collimated outflows could face some difficulties in explaining large event rates (i.e. $\approx 1/100$ of the supernova rate). On the other hand, one appealing aspect of massive star progenitors is that the large variety of stellar parameters could explain the diversity of jet opening angles. If however the GRB 980425/1998bw association is real, then we may have a new class of GRB with lower energy $E_\gamma \approx 10^{48}(\Omega_j/4\pi)$ erg, which is only rarely observable even though its comoving density could be substantial.

2.2 *Anisotropic relativistic outflows*

Broader jets can also be produced by a magneto rotational mechanism, however, some concern has been raised that these outflows may not be easily accelerated to $\Gamma > 10$ (Meier et al. 2001 and references therein). Detailed predictions are nonetheless still in need of three dimensional, high-resolution core-collapse calculations. Other mechanisms of jet production such as neutrino radiation in the context of the collapsar model (MacFadyen & Woosley 1999) or intense radiation of a newly born pulsar (Blackman & Yi 1998) could be less constraining in their beaming

requirements.

If the large variety of behaviors exhibited from burst to burst is produced by viewing an anisotropic universal beam configuration from different directions, the opening angle of the jet $\theta_j > \theta_v$ should still affect the light curve at the time when the edge of the jet becomes visible (this break would be additional to the one predicted from the viewing angle dependence; Rossi et al. 2002, Zhang & Mészáros 2002). If the critical Lorentz factor is less than 3 or so (the opening angle exceeds 20°) such a transition might be masked by the transition from ultra relativistic to mildly relativistic flow, so quite generally it would be difficult to limit the opening angle of this anisotropic outflow if it exceeds 20° . Although, the jet sideways expansion in this model is likely to be very important and more detailed calculations are required in order to understand the exact shape of the afterglow light curve, it is nonetheless important to mention that some afterglows are unbroken power laws for over 100 days (e.g. GRB 970228), implying that the opening angle of the late-time afterglow at long wavelengths is probably $> 20^\circ$.

Also, under this interpretation, the γ -rays are likely to be more narrowly beamed than the optical afterglow and therefore there should be many “orphan” afterglows. The transient sky at faint magnitudes is poorly understood, but there are two major searches to find supernova down to $R=23$ (Garnavich et al. 1998; Perlmutter et al. 1998). These searches are sensitive to afterglows of the brightness levels observed to date and have covered a few tens of square degree years of exposure. It then follows that the afterglow rate is not more than a few times $0.1/\text{sq deg/yr}$. Considering that the magnitude limit of these searches allows optical counterparts brighter than $1 \text{ ph cm}^{-2} \text{ s}^{-1}$ to be detected, the ratio of orphan afterglows to GRB is unlikely to exceed ≈ 10 (Mészáros, Rees & Wijers 1999). This condition is not in disagreement with the few number of orphan afterglows that are predicted from an anisotropic universal beam configuration (Rossi et al. 2002). Studies of the transient sky at magnitudes down to $R \approx 25$ should be able to disprove or consolidate this anisotropic model. The location of GRBs within their parental galaxy could help settle this question, since recently it was suggested that bursts located closer to the center of their parent galaxies have smaller isotropic equivalent energies (Ramirez-Ruiz, Lazzati & Blain 2002). If confirmed in further host observations, this correlation will strongly complicate this universal beam interpretation. A direct test of this model remains, however, the time dependent measurements of polarization.

3 Internal Shocks: A Phenomenological Study

3.1 Model Outline

We simulate GRB light curves by adding pulses radiated in a series of internal shocks that occur in a transient, unsteady relativistic wind (Rees & Mészáros 1994). Several authors have modeled this process by randomly selecting the initial conditions at the central site (Kobayashi et al. 1997; Daigne & Mochkovitch 1998; Pilla & Loeb 1998; Panaitescu, Spada, Mészáros 1999, Spada, Panaitescu & Mészáros 2000; Ramirez-Ruiz, Merloni & Rees 2001). The model used here is similar to that described by Ramirez-Ruiz et al. (2001) but differs in the following aspects: (i) Our treatment of the radiation emission takes into account synchrotron emission and Compton scattering; (ii) The effect of photon diffusion through the optically thick wind is included, which may be very important in obscuring pulses that occur at small radii; (iii) We use the shock jump equations to determine the physical conditions in the shocked fluid, and (iv) The duration of the pulse width Δt_0 is calculated by adding in quadrature the angular spreading time $\Delta T_a \approx R/(2\Gamma^2 c)$, the radiative cooling time $\Delta T_r \approx t_\gamma/\Gamma$ (where t_γ is the lab-frame radiative timescale), the shell crossing time $\Delta T_\Delta \approx t_\Delta/\Gamma^2$ (where $t_\Delta \approx \Delta/|v_{\text{sh}} - v_0|$ is the lab-frame shock's crossing time, v_{sh} is the shell preshock flow velocity and Δ is the shell thickness) and the diffusion time ΔT_d through the optically thick wind as done by Panaitescu et al. 1999 and Spada et al. 2000.

The wind is discretized into a sequence of $N = T_{\text{dur}}/\overline{\delta t_i}$ shells with a range of initial thickness Δ_i , where T_{dur} is the duration time of the wind ejection from the central source and $\overline{\delta t_i} \ll T_{\text{dur}}$ is the average interval between consecutive ejections. The time interval δt_i between two consecutive ejections i and $i+1$ is assumed to be proportional to the $i+1$ th shell energy. This implies that longer periods of quiescence, during which the engine accumulates fuel, are followed by more energetic shells (this is motivated by the observations of Ramirez-Ruiz & Merloni 2001 and Nakar & Piran 2002). The different values of δt_i are selected from the log normal distribution of pulse intervals found by Norris et al. (1996).

We calculate the radii where shells collide and determine the emission features for each pulse. If some inner shell moves faster than an outer one ($\Gamma_i > \Gamma_j$), it will overtake the slow one at a radius $R_i(t_{ij}) = R_j(t_{ij}) = R_c \propto \Gamma_i^2$. For each collision between two shells there is a reverse and a forward shock. The shock jump equations determine the physical parameters of the shocked fluids: the velocities of the shock fronts, the internal energy in the shocked fluid frame u' , and both the thickness Δ_{ij} and Lorentz factor Γ_{ij} of the merged shell at the end of the collision. We assume that in between two consecutive collisions the thickness of the shell increases proportionally to the fractional increase of its radius $\frac{d\Delta_i}{\Delta_i} \propto \frac{dR}{R}$ (e.g. Spada et al. 2000). The ejection parameters determine the dynamics of the wind and the dynamical efficiency, ϵ_{ij} . This efficiency reflects the differences between the Lorentz factors of a pair of colliding shells. The efficiency for an individual collision can be calculated

from the initial and final bulk energies,

$$\epsilon_{ij} = 1 - \frac{M_{ij}\Gamma_{ij}}{M_i\Gamma_i + M_j\Gamma_j} \quad (3)$$

where

$$\Gamma_{ij}^2 = \Gamma_i\Gamma_j \frac{M_i\Gamma_i + M_j\Gamma_j}{M_i\Gamma_j + M_j\Gamma_i}, \quad (4)$$

and the resulting mass is $M_{ij} = M_i + M_j$. The first collisions remove the initial random differences between the Lorentz factors of successive shells. If the mean Lorentz factor $\bar{\Gamma}$ remains steady for the entire burst duration, then the efficiency steadily decreases during the wind expansion. If $\bar{\Gamma}$ is modulated on a timescale much smaller than the overall duration of the wind, dynamically efficient collisions at large radii are still possible.

A fraction $\zeta \leq 1$ of the shock-accelerated electrons is assumed to have a power law distribution $-p$ in the electron Lorentz factor γ_e , starting from a low random Lorentz factor $\gamma_m \approx \frac{1}{3} \frac{m_p}{m_e} \frac{\epsilon_e}{\zeta} (\Gamma'_{ij} - 1)$, where the energy stored in electrons is a fraction ϵ_e , Γ'_{ij} is the Lorentz factor for internal motions in the shocked frame and we assume $p = 2.5$. The magnetic field is assumed to be turbulent and parameterized through the fraction ϵ_B of the internal energy it contains: $B^2 \approx 8\pi\epsilon_B u'$ (primed quantities are measured in the comoving frame). The synchrotron spectrum of each pulse is approximated as three power-law segments, with the high energy slope(s) depending on p and the relative values of the peak and cooling frequencies. The typical energy of synchrotron photons as well as the synchrotron cooling time depend on the Lorentz factor γ_e of the accelerated electrons and on the strength of the magnetic field. The two energy release parameters ζ and ϵ_B alter the peak energies of the synchrotron and inverse Compton spectra (they are higher for lower ζ) and the Comptonization parameter (which is larger for smaller ϵ_B).

The shock-accelerated electrons radiate, and the emitted photons can be upscattered on the hot electrons ($\gamma_e \gg 1$) or downscattered by the cold ones ($\gamma_e \approx 1$). The optical depth to upscattering, far from the Klein-Nishina regime, is $\tau_{ic}\sigma_{Th}\zeta n'_e \min(ct'_\gamma, \Delta')$ (Spada et al. 2000), where n'_e is the electron density and $t'_\gamma = t'_{sy}/(1+y)$ is the radiative timescale with t'_{sy} the synchrotron cooling time and y the Comptonization parameter ($y = \gamma_m^2 \tau_{ic}$ for $\tau_{ic} < 1$). A fraction $\min(1, \tau_{ic})$ of the synchrotron photons is inverse Compton scattered $n_{ic} = \max(1, \tau_{ic}^2)$ times unless the Klein-Nishina regime is reached (Panaitescu et al. 1999). The energy of the upscattered photons is $h\nu_{ic} = \min[\gamma_m m_e c^2, h\nu_{syn}(4\gamma_m^2/3)^{n_{ic}}]$. The optical thickness τ_c for the cold electrons within the emitting shell is calculated by taking into account the cold electrons within the hot fluid - those that were accelerated but have cooled radiatively while the shocked crossed the shell- and those within the yet unshocked part of the shell. When $\tau_c > 1$, photons are downscattered by the cold electrons before they escape the emitting shell, leading to a decrease in photon energy and increase in

photon duration. We approximate the increase in pulse duration due to the diffusion through optically thick shells by the time ΔT_d it takes for a photon to diffuse through them (Spada et al. 2000). The addition of all pulses gives both the burst spectra and the gamma-ray light curve. The latter is binned on a timescale of 64 ms and is used to compute the burst variability, that is, the average mean-square of the count variations relative to a smoothed time profile (calculated using a boxcar function with a timescale equal to 30% of the duration that contains 90% of the total counts; see Fenimore & Ramirez-Ruiz 2002a). A simulated profile depends on the specific values of the relevant model parameters describing the wind ejection ($N \approx 50$, δt_i , Γ_{\max} , and Γ_{\min}) and the radiative efficiency of the pulses (ϵ_e , ζ and ϵ_B).

3.2 On the internal structure of the relativistic wind

We study the effects of varying the energy per unit solid angle of the expelled outflow by an increase either in the bulk Lorentz factor or in the baryon loading. One simple possibility is that the central engine ejects consecutive shells in which the Lorentz factors Γ_i are randomly selected between Γ_{\min} and Γ_{\max} . The shell mass M is then assumed constant and determined by the wind isotropic equivalent energy by requiring that $Mc^2 = E_{4\pi} / \sum_{i=1}^N \Gamma_i$. In this scenario, narrow jets (or jets viewed close to the jet axis) should have higher Lorentz factors. Assuming $\Gamma_{\max} \propto \theta_{j,v}^{-2}$, then $E_{4\pi} \propto \Gamma_{\max}$ (Kobayashi et al. 2002). Nonetheless, it could be also possible that changes in the energy per unit solid angle are mainly caused by variations in the baryon loading of the wind. In this case, the average bulk Lorentz factor $\bar{\Gamma} = \Gamma_{\min}/2 + \Gamma_{\max}/2$ remains unchanged throughout the entire wind and equal to $\bar{\Gamma} = E_{4\pi} / \sum_{i=1}^N M_i c^2$ with M_i randomly drawn from the interval $[M_{\min}, M_{\max}]$ (the shell Lorentz factors Γ_i are random between $\bar{\Gamma} - \Delta\bar{\Gamma}$ and $\bar{\Gamma} + \Delta\bar{\Gamma}$). Assuming a correlation between M_{\max} and $\theta_{j,v}$, then $E_{4\pi} \propto M_{\max}$. These two extreme scenarios will be referred to in the following as *impulsive* and *lethargic* outflows, respectively.

3.3 Impulsive outflows

To simulate the effects of an *impulsive* outflow, we calculate the temporal and spectral profiles of 10^2 realizations for a given Γ_{\max} , which we used to evaluate the peak of the spectrum in νF_ν and the mean variability. The wind (isotropic equivalent) energy, in all cases, is drawn from a log normal distribution with an average value $\overline{E_{4\pi}} = 10^{54} (\Gamma_{\max}/10^3)$ erg and a dispersion $\sigma_E = 10^{1/3}$ erg. Numerous collisions happen during the evolution of the wind. Each collision produces a pulse, whose strength strongly depends on Γ_{\max} , since the wind luminosity increases with Γ_{\max} .

The optical thickness τ_c is determined mainly by the wind luminosity, $L_w = E_{4\pi}/T_{\text{dur}}$, and the range of Lorentz factors in the wind. For small collision radii $R \propto \Gamma^2$, the

pulse duration is dominated by the time it takes the photon to propagate through all the shells of optical thickness above unity. Thus, photons are downscattered by the cold electrons before they escape the wind, leading to an increase of the pulse width and a decrease in the photon energy - photon diffusion through the wind widens pulses that would otherwise would appear narrow since they occur at small radii (Figure 2). This would be the case when the typical Lorentz factor Γ_i is relatively small. The smoothing effect is expected to be stronger when the density of scattering is amplified by new e^\pm pairs are formed in the originally thick scattering medium (Thompson & Madau 2000; Guetta, Spada & Waxman 2001; Mészáros, Ramirez-Ruiz & Rees 2001; Beloborodov 2002). For larger radii, the pulse duration is dominated by both shell crossing and radiative timescales (Figure 2), which decrease as Γ_i increases (ΔT_Δ increases as a result of the shell widening, while ΔT_r is larger for later collisions because B and γ_m are lower). The latter timescale is found to be comparable to the angular spreading one during the whole wind expansion, for the assumed linear shell-broadening between collisions. This implies that for large Lorentz factors, internal collisions will produce pulses with small ΔT_0 and high $E_{4\pi}$ - giving rise to a very spiky and luminous light curve.

By running models with 10^2 different values of Γ_{\max} ranging from 100 to 3×10^3 (assuming $\Gamma_{\max}/\Gamma_{\min}=20$), we have found that more variable profiles ($> \Gamma_{\max}$) have higher luminosities and can reasonably fit the observational data (see Figure 3, where the shaded region depict the 1σ region). The variability reaches an asymptotic value around $V \approx 0.1$ because the light curve is binned on a timescale of 64 ms to compare with BATSE temporal resolution. On the other hand, for very low radii (small Γ_{\max}), the first collisions remove the initial random differences between the Lorentz factors of successive shells before reaching the radius of transparency. As a result, the efficiency steadily decreases during the wind expansion giving rise to very under luminous burst in which the variability measurement saturates due to count statistics. In this particular example, the values of the ejecta Lorentz factors are such (i.e. $\Gamma_{\max}/\Gamma_{\min}$ is set to be constant) that the average efficiency of individual collisions $\bar{\epsilon}_{ij}$ is independent of the intrinsic luminosity of the outflow (or Γ_{\max}). Within our model more efficient collisions can alternatively be produced by increasing Γ_{\max} , while leaving Γ_{\min} unchanged. The difference in the shell Lorentz factors (i.e. Γ_{ij}) in this case will be much larger, giving rise to more luminous pulses than in the previous case. A smaller range of Γ_{\max} values is thus required to produce similar changes in the burst isotropic luminosity (see the banded region in Figure 3). The numerical results shown in Figure 3 assume that the fraction ϵ_B is distributed uniformly in logarithmic space between 10^{-2} and 10^{-1} , $n_{\text{ISM}} = 1 \text{ cm}^{-3}$ (in this case most collisions take place before the deceleration radius of the wind; see Fenimore & Ramirez-Ruiz 2002b), $\epsilon_e = 0.25$ and that $\zeta \approx 0.1$.

The process by which the dissipated energy is finally radiated depends on the energy distribution of protons and electrons in the shocked material and on the values of the comoving density and magnetic field. The internal shocks heat the expanding

ejecta, amplifying the preexisting magnetic field or generating a turbulent one, and accelerate electrons, leading to synchrotron emission and inverse Compton scattering. By varying the injection fraction ζ one can study the relative intensity of the synchrotron and inverse Compton components and determine those values that maximize the received flux in the BATSE range. For $\zeta > 10^{-2}$ the inverse Compton emission occurs in the Thomson regime and carries most of the burst energy in the BATSE window, while for $\zeta < 10^{-3}$ synchrotron dominates over inverse Compton scattering as the latter takes place in the Klein-Nishina regime (Panaitescu et al. 1999). Figure 4 shows the evolution of the synchrotron (which for $\zeta=1$ lies mainly below the BATSE window) and inverse Compton peaks before and after downscattering for both thick and a thin winds. For smaller collision radii (i.e. small Γ_{\max}), the emission takes place where the wind is optically thick, leading to a decrease in the photon energy - diffusion through the wind decreases the photon energy that would otherwise would appear large since they are produced at small radii where B is larger. For the set of parameters considered here, the Thompson limit is usually a good approximation to treat the downscattering of the synchrotron photons. The inverse Compton emission, however, peaks at large comoving frame energies, and the general cross section has to be considered. For these energetic photons, the cross section strongly depends on the photon energy and varies after each photon interaction. Figure 5 shows the shifting of the burst emission towards higher energies with increasing variability, due to the increase of Γ_{\max} from 100 to 3×10^3 and assuming $\Gamma_{\max}/\Gamma_{\min}=20$ (corresponding to the internal shock parameters of the simulations shown in Figure 3). This increase in energy stops once the average bulk Lorentz factor is large enough that collisions take place where the wind is optically thin (see the shaded region in Figure 5). The typical radiation energy of each pulse also strongly depends on the resulting Lorentz factor Γ_{ij} . Thus it is possible to produce a larger dynamic range of spectral peak energies by increasing Γ_{\max} , while leaving Γ_{\min} unchanged (see banded region in Figure 5). We found that more variable profiles have higher spectral peaks and can reasonably fit the observational data (Lloyd-Ronning & Ramirez-Ruiz 2002) provided that $\zeta > 10^{-2}$. In this case, the synchrotron emission lies mainly below the BATSE window and the inverse Compton component carries most of the energy of burst. When synchrotron emission dominates over inverse Compton scattering, as the latter takes place in the Klein Nishina regime (i.e. $\zeta < 10^{-2}$), we find that simply varying Γ_{\max} of the shells does not produced the dynamical range of peak energies that is observed. This is mainly because the typical observed synchrotron frequency, which at R_c gives

$$h\nu_{\text{syn}} \propto \frac{\epsilon_e^2 \epsilon_B^{1/2} (\Gamma'_{ij} - 1)^2 L_w^{1/2}}{R_c (1+z)}, \quad (5)$$

is unlikely to increase by simply incrementing Γ as $R_c \propto \Gamma^2$ gives $h\nu_{\text{syn}} \propto \Gamma^{-2}$ for a constant L_w , ϵ_B , ϵ_e and Γ'_{ij} . Assuming the correlation between the Lorentz factor and $\theta_{j,v}$, the isotropic energy itself is related to the source expansion velocity,

$L_w \propto E_{4\pi} \propto \Gamma_{\max}$, and the typical observed synchrotron frequency is then $\nu \propto \Gamma^{-3/2}$. This may be overcome by implicitly assuming that the electrons are continually accelerated in the shocked region (see Lloyd & Petrosian 2000) or by postulating that the equipartition energy acquired by the electrons and the magnetic field (ϵ_e and ϵ_B) are dependent on Γ . While these are strong constraints in the emission properties, it is worthy of notice that the correlation between variability and spectral energy could be significantly affected by selection effects and more GRBs with independent spectroscopic redshifts are need it in order to test its validity (Lloyd-Ronning & Ramirez-Ruiz 2002). This relationship -if true- can help shed light on the relevant emission mechanisms in unsteady outflows. We would also like to emphasize that the wind optical thickness is one of the factors to which the variability and spectral peak energy is most sensitive. Indeed, it is reassuring that the inclusion of this effect is of the utmost importance to reproduce the power density spectrum of gamma-ray bursts arising from internal shocks in unsteady outflows (Panaitescu et al. 1999, Spada et al. 2000).

3.4 Lethargic outflows

Until this point we have assumed that the changes in the energy per unit solid angle are caused solely by an increase in the bulk Lorentz factor ($M=\text{constant}$). Nonetheless, it could be possible that changes in $E_{4\pi}$ may be mainly caused by variations in the baryon loading of the wind. We have run such *lethargic* models and find that simply varying the baryon loading of the wind of the ejected shells does not reproduce the dynamic range of variability and spectral energies that is observed. We also study intermediate behaviors by assuming that the shell baryon loading and its Lorentz factor are related: $\Gamma \propto M^\alpha$. We conclude that, within such models, the burst phenomenology can be accommodated provided that the changes in the energy per unit solid angle within different beams is dominated by Γ with $\alpha < 0.2$. This is not surprising since the timescales that determine the pulse structure and thus the variability are highly dependent on $R_c \propto \Gamma_i^2$. An interesting consequence is that large variations in the energy per unit solid angle within different beam models should be strongly dominated by changes in Γ .

4 Discussion

The main conclusion we can draw from the simulations presented above is that, in the framework of the internal shocks model, there are realistic assumptions in

⁴ This scaling is valid if ϵ_B , ϵ_e and Γ'_{ij} are constant. However, it is possible to produce a larger dynamical range of spectral energies by increasing Γ_{\max} while leaving Γ_{\min} unchanged. In this case, $\Gamma'_{ij} \propto \Gamma$ and thus $h\nu_{\text{syn}} \propto \Gamma^{1/2}$

which the variable activity of GRB is found to be correlated with absolute peak luminosity. We attribute this correlation to a variation of the energy per unit solid angle caused mainly by an increase in the emitting regions' Lorentz factors in the context of *impulsive* relativistic outflows. This change of the Doppler factor could be attributable either to a standard type of event viewed from different orientations or by changes in the collimation of GRBs jets. Within such models, collisions between shells with higher Lorentz factors, which are intrinsically more luminous, produce more variable profiles. The existence of a correlation between the characteristic photon energy in the cosmological rest frame and the GRB variability, on the other hand, imposes more constraining requirements. The main characteristics of the modeled bursts with the above mentioned features are: a high electron injection fraction – which implies that the inverse Compton scattering dominates over synchrotron emission – required to increase the spectral peak energy of the larger collision radii; and a wind optical thickness to scattering on cold electrons above unity is required to increase the duration of the pulses and decrease the photon energy of the collisions that take place at smaller radii.

We must also remain aware of other possibilities. For instance, we may be wrong in supposing that the main radiation mechanism assumed to be responsible for the burst event is synchrotron or its inverse Compton component. It could be that the GRB emission originates from a fireball moving out through an extended stellar envelope, along a funnel that is empty of matter but pervaded by thermal radiation from the funnel walls, leading to Compton drag (Lazzati et al. 1999; Ghisellini et al. 2001). The fireball itself remains optically thick until it expands beyond the stellar surface (see also Ramirez-Ruiz, MacFadyen & Lazzati 2002). A burst with complex time-structure could then be produced by a series of expanding shells. In this scenario, faster moving shells will produce greater peak energies, as the burst emission simply reflects the temperature of the funnel photons up-scattered by the square of the bulk Lorentz factor. Furthermore, these fast shells will produce both smaller and more luminous pulses. This is because the observed variability timescale, which is related to the typical size of the region containing the dense seed photon divided by the time compression factor, increases with Γ and the Compton drag is more efficient for faster shells. To this end, ejection of very rapid shells will lead to bursts produced by the ejection of very rapid shells are both more variable and have larger peak spectral energies.

Much progress has been made in understanding how afterglows can arise from a forward shock or blast-wave moving into the external medium ahead of the ejecta, and in deriving the generic properties of the long wavelength afterglows that follow from this (Mészáros 2001). There still remain a number of mysteries, especially regarding the prompt emission, in particular, the formation of the ultra relativistic outflow, its structure and the radiation process. As we have shown, the correlations between the characteristic photon energy, the gamma-ray burst variability and its

luminosity, as well as the jet collimation, can help shed light on all three of these issues.

Acknowledgements

We are indebted to M. J. Rees and D. Lazzati for very useful discussions. We thank D. Lazzati for highlighting the relevance of the Compton drag scenario in reproducing the burst phenomenology. We would also like to thank E. Fenimore, S. Kobayashi, P. Kumar, A. Panaitescu, E. Rossi and the referee P. Mészáros for helpful insight regarding internal-shock and non-thermal radiation calculations. ERR acknowledges support from CONACYT, SEP and the ORS foundation.

References

- Aloy, M. A., Ibanez, J. M., Marti, J. M., Muller E., & MacFadyen A. I., 2000, *ApJ*, 531, L119
- Amati, L., et al., 2000, *Science*, 290, 953
- Antonelli, A., et al., 2000, *ApJ*, 545, L39
- Ballantyne, D., & Ramirez-Ruiz, E., 2001, *ApJ*, 559, L83
- Beloborodov, A. M., 2002, 565, 808
- Berger, E., Kulkarni, S. R., Frail, D. A., 2001, *ApJ*, 560, 652
- Björnsson, G., Hjorth, J., Jakobsson, P., Christensen, L., Holland, S., 2001, *ApJ*, 552, L121
- Blackman, E. G., & Yi, I., 1998, *ApJ*, 498, L31
- Blandford, R. D., & Znajek, R., 1977, *MNRAS*, 179, 433
- Bloom, J. S., et al., 1999, *Nature*, 401, 453
- Böttcher, M., & Fryer, C. L., 2001, *ApJ*, 547, 338
- Castro-Tirado, A. J., et al., 1999, *Science*, 283, 5410, 2069
- Chevalier, R. A., & Li, Z.-Y., 2000, *ApJ*, 536, 195
- Costa, E., et al., 1997, *Nature*, 387, 783
- Daigne, F., & Mochkovitch, R., 1998, *MNRAS*, 296, 275.
- Fenimore, E. E., & Ramirez-Ruiz, E., 2002a, *ApJ*, submitted (astro-ph/0004176)
- Fenimore, E. E., & Ramirez-Ruiz, E., 2002b, *ApJ*, submitted (astro-ph/astro-ph/9909299)
- Frail, D. A., et al., 1997, *Nature*, 389, 261
- Frail, D. A., et al., 2001, *ApJ*, 562, L55
- Fruchter, A. S., et al, 1999, *ApJ*, 520, 54
- Galama, T. J., et al., 1998, *Nature*, 395, 670
- Garnavich, P. et al., 1998, *ApJ*, 493, L53

Ghisellini, G., Lazzati, D., Celotti, A., & Rees, M. J., 2001 MNRAS, 316, L45
 Guetta, D., Spada, M., & Waxman, E., 2001, ApJ, 557, 399
 Harrison, F. A., et al., 1999, ApJ, 523, L121
 Huang, Y. F., Dai, Z. G., & Lu, T., 2000, MNRAS, 316, 943
 Ioka, K., & Nakamura, T., 2001, ApJ, 554, L163
 Khokhlov, A. M., et al., 1999, ApJ, 529, L107
 Kobayashi, S., Piran, T., & Sari, R., 1997, ApJ, 490, 92
 Kobayashi, S., Ryde, F., & MacFadyen, A. I., 2002, ApJ, in press (astro-ph/0110080)
 Kulkarni, S. R., et al., 1998, Nature, 395, 663
 Kulkarni, S. R., et al., 1999, Nature, 398, 389
 Lazzati, D., Campana, S., & Ghisellini, G., 1999, MNRAS, 304, L31
 Lazzati, D., Ghisellini, G., Celotti, A., & Rees, M. J., 2000, ApJ, 529, L17
 Lazzati, D., Ghisellini, G., Amati, L., Frontera, F., Vietri, M., & Stella, L., 2001a, ApJ, 556, 471
 Lazzati, D., et al., 2001b, A&A, 378, 996
 LeBlanc, J. M., & Wolson, J. R., 1970, ApJ, 161, 541
 Lloyd, N.M., & Petrosian, V., 2000, ApJ, 543, 722
 Lloyd-Ronning, N. M., & Ramirez-Ruiz, E., 2001, ApJ in press (astro-ph/0205127)
 MacFadyen, A. I., & Woosley, S. E., 1999, ApJ, 524, 262
 MacFadyen, A. I., Woosley, S. E., & Heger, A., 2001, ApJ, 550, 410
 Meier, D. L., et al., 1976, ApJ, 204, 869
 Meier, D. L., Koide, S., & Uchida, Y., 2001, Science, 291, 84
 Mészáros, P., 2001, Science, 291, 79
 Mészáros, P., & Rees, M. J., 1997, ApJ, 476, 232
 Mészáros, P., Rees, M. J., & Wijers, R. A. M. J., 1998, NewA, 4, 301
 Mészáros, P., Ramirez-Ruiz, E., & Rees, M. J., 2001, ApJ, 554, 660
 Nakar, E. & Piran, T., 2002, MNRAS, 331, 40
 Norris, J. P., 2002, ApJ, submitted (astro-ph/0201503)
 Norris, J. P., et al., 1996, ApJ, 459, 2393
 Norris, J. P., Marani, G. F., & Bonnel, J. T., 2000, ApJ, 534, 248
 Paczyński, B., 1998, ApJ, 494, L45
 Panaitescu, A., Spada, M., & Mészáros, P., 1999, ApJ, 522, L105
 Panaitescu, A., & Kumar, P., 2001, ApJ, 554, 667
 Perlmutter, S., et al., 1998, Nature, 391, 51
 Pilla, R. P., & Loeb, A., 1998, 494, L167
 Piran, T., 1999, Physics Reports, 314, 575
 Piran, T., Kumar, P., Panaitescu, A., & Piro, L., 2001, ApJ, 560, L167
 Piro, L., et al., 1999, ApJ, 514, L73
 Piro, L., et al., 2000, Science, 290, 955
 Plaga, R., 2001, A&A, 370, 351
 Ramirez-Ruiz, E., & Merloni, A., 2001, MNRAS, 320, L25
 Ramirez-Ruiz, E., Merloni, A., & Rees, M. J., 2001, MNRAS, 324, 1147
 Ramirez-Ruiz, E., Dray, L., Madau, P., & Tout, C. A., 2001, MNRAS, 327, 829
 Ramirez-Ruiz, E., Lazzati, D., & Blain, A. W., 2002, ApJ, 565, L9

Ramirez-Ruiz, E., MacFadyen, A. I., & Lazzati, D., 2002, MNRAS, 313, 197
Rees, M. J., 1999, A&AS, 138, 491.
Rees, M. J., & Mészáros, P., 1994, ApJ, 430, L93
Rees, M. J., & Mészáros, P., 2000, ApJ, 545, L73
Reichart, D. E., 1999, ApJ, 521, L111
Rhoads, J. E., 1997, ApJ, 487, L1
Rossi, E., Lazzati, D., & Rees, M. J., 2002, MNRAS, 332, 945
Salmonson, J. D., 2001, ApJ, 544, L115
Salmonson, J. D., & Galama T. J., 2002, ApJ, 569, 682
Spada, M., Panaitescu, A. & Mészáros, P., 2000, ApJ, 537, 824.
Stern, B., Poutanen, J., & Svensson, R., 1997, ApJ, 489, L41
Thompson, C., & Madau, P., 2000 ApJ, 538, 105
Uchida, Y., & Shibata, K., 1985, PASJ, 37, 515
van Paradijs, J., et al., 1997, Nature, 386, 686
Vietri, M., 1997, ApJ, 478, L9
Vietri, M., Ghisellini, G., Lazzati, D., Fiore, F., & Stella, L., 2000, ApJ, 550, L43.
Woosley, S. E., 1993, ApJ, 405, 273
Wheeler, J. G., Yi, I., Hoflich, P., & Wang, L., 1999, ApJ, 537, 810
Yoshida, A., et al., 1999, A&AS, 138, 433.
Zhang, B., & Mészáros, P., 2002, ApJ, 571, 876

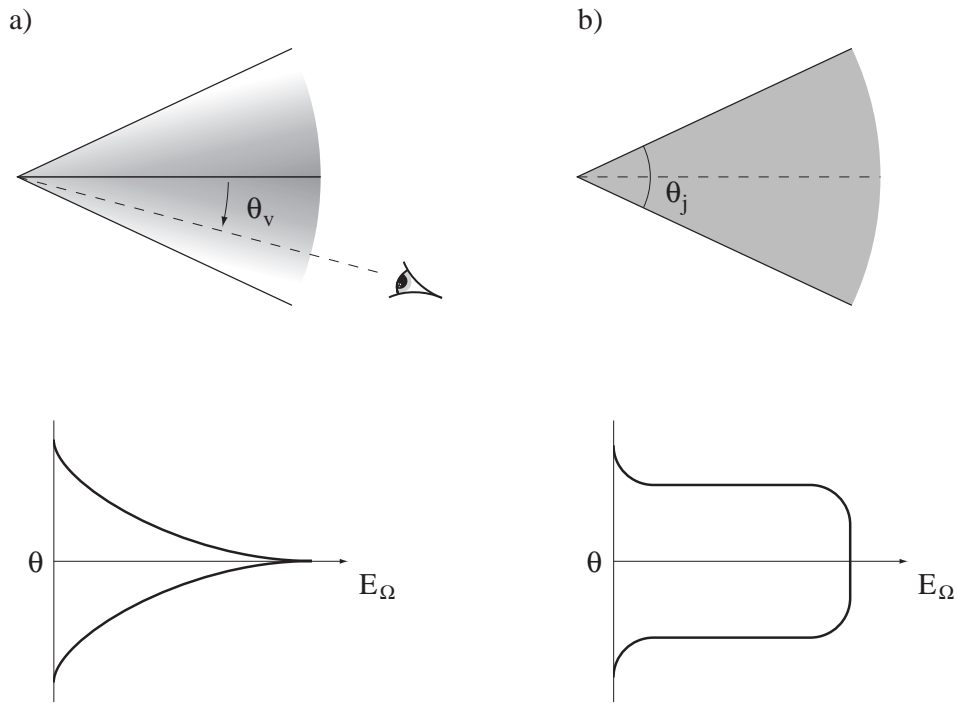


Fig. 1. Diagram illustrating two different configurations of beaming models. The GRB phenomenology could be attributable either to a standard type of event with an axisymmetric energy distribution of the form $E(\theta_v) \propto \theta_v^{-\beta}$ viewed from different orientations (a) or to a standard energy reservoir but with a variety of beaming angles (b).

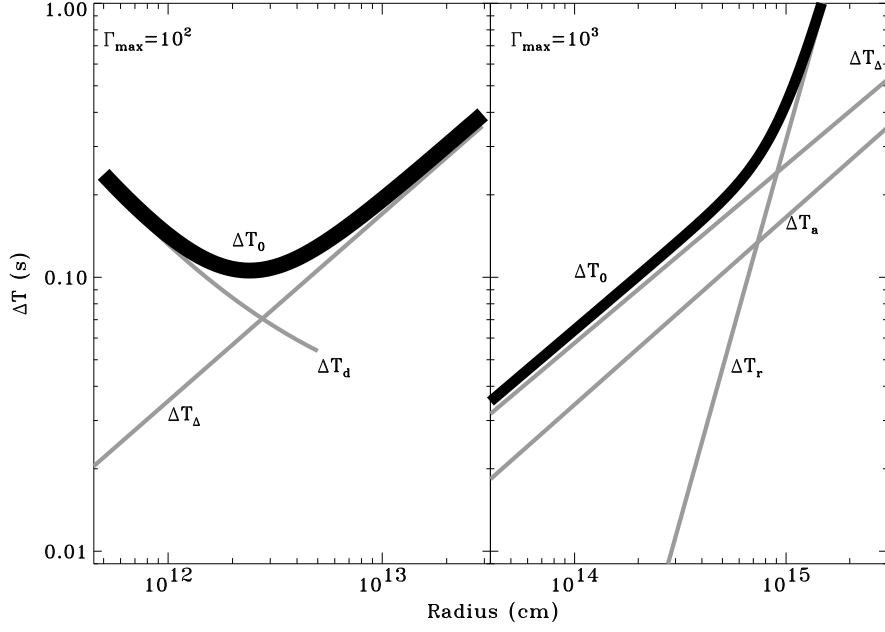


Fig. 2. Evolution of the pulse duration as a function of the radius of collision and of the timescales that contribute to it. For lower Lorentz factor $\Gamma_{\max} \approx 10^2$ the collisions take place at smaller radius where the wind is optically thick, photons are down scattered by the cold electrons before they escape, leading to an increase of the pulse duration $\Delta T_d \approx \Delta T_0$ and a decrease of the pulse energy. For $\Gamma_{\max} \approx 10^3$ most collisions occur where the shells are optically thin $\Delta T_d \ll \Delta T_0$. The radiative cooling time is negligible with respect to ΔT_a and ΔT_Δ for collisions occurring at small radii, while for very large radii (i.e. small number of collisions) ΔT_r is the dominant contribution.

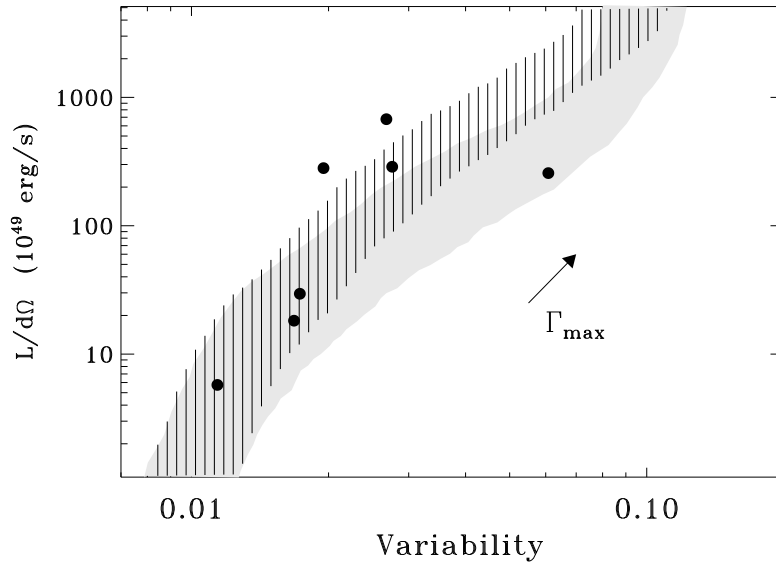


Fig. 3. The luminosity per unit solid angle as a function of variability for bursts arising from multiple shock in a relativistic wind. The filled circles are bursts with secure redshifts estimates (Fenimore & Ramirez-Ruiz 2002a). The shaded area and banded areas represent the 1σ regions of two different sets of random simulations. The former shows the effect of increasing $\Gamma_{\max}/\Gamma_{\min}$, while the latter depicts the effect of increasing Γ_{\max} but leaving Γ_{\min} unchanged. The observed trend reproduced as bursts with higher source expansion velocity, which are intrinsically more luminous, produce more variable temporal profiles.

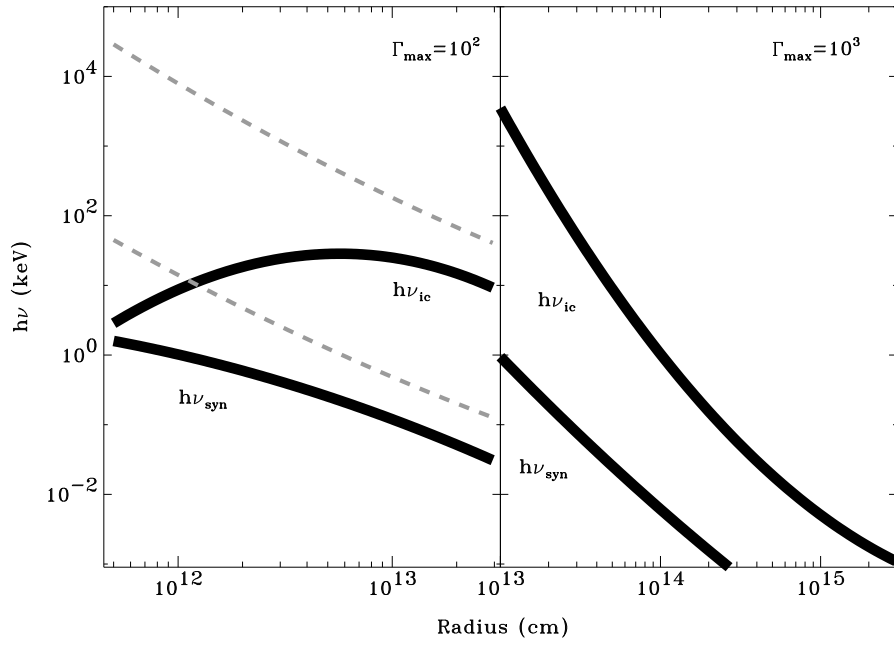


Fig. 4. Downscattered synchrotron and inverse Compton energy peaks as a function of the radius of collision. The dash lines represent the evolution of the spectral peak of these two emission components before downscattering ($\epsilon_e = 0.25$, $\epsilon_B = 0.1$, and $\zeta = 1$). For collisions taking place at smaller radii (left panel), the wind is optically thick and photons are downscattered by the cold electrons before they escape the wind.

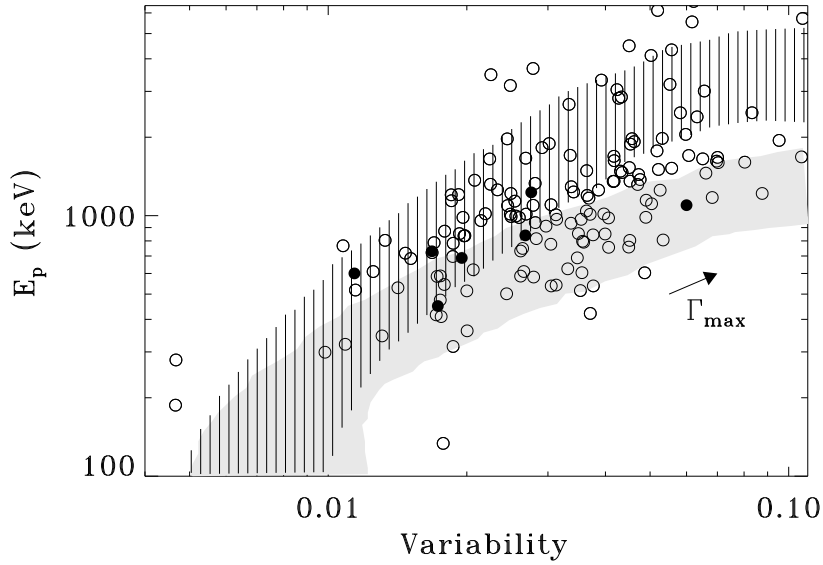


Fig. 5. The peak of the νF_ν spectrum as a function of variability for bursts arising from an unsteady relativistic wind. The filled circles are bursts with secure redshifts estimates, while the empty circles are bursts in which the redshift is derived using the variability-luminosity distance indicator (Lloyd-Ronning & Ramirez-Ruiz 2002). The shaded and banded areas represent the 1σ regions corresponding to the internal shock parameters of the simulations shown in Figure 3. Again, the observed trend is reproduced, as bursts with higher source expansion velocity, which are intrinsically more luminous, radiate photons with higher characteristic energies after diffusion through the optical wind has taken place.